CNS Neuroscience & Therapeutics

ORIGINAL ARTICLE

CNS Neuroscience & Therapeutics

Epicentral Disruption of Structural Connectivity in Alzheimer's Disease

Carlo Augusto Mallio,[1] Ruben Schmidt,[2] Marcel A. de Reus,[3] Fabrizio Vernieri,[4] Livia Quintiliani,[4] Giuseppe Curcio,[5] Bruno Beomonte Zobel,[1] Carlo Cosimo Quattrocchi[1] & Martijn P. van den Heuvel[3]

1 Departmental Faculty of Medicine and Surgery, Unit of Diagnostic Imaging, Università Campus Bio-Medico di Roma, Rome, Italy
2 Brain Center Rudolf Magnus, Department of Neurology, University Medical Center Utrecht, Utrecht, the Netherlands
3 Brain Center Rudolf Magnus, Department of Psychiatry, University Medical Center Utrecht, Utrecht, the Netherlands
4 Departmental Faculty of Medicine and Surgery, Unit of Neurology, Università Campus Bio-Medico di Roma, Rome, Italy
5 Department of Life, Health and Environmental Sciences, University of L'Aquila, L'Aquila, Italy

Keywords
Alzheimer's Disease; Connectivity; Connectome; Diffusion-weighted imaging; Epicentral disruption; Mild cognitive impairment.

Correspondence
C. Augusto Mallio, MD, Unit of Diagnostic Imaging, Università Campus Bio-Medico di Roma, Via Álvaro del Portillo 21, 00128 Rome, Italy.
Tel.: +39-6-225411708;
Fax: +39-6-22541456;
E-mail: c.mallio@unicampus.it
Received 21 November 2014; revision 26 February 2015; accepted 13 March 2015

SUMMARY

Aims: Neurodegenerative changes observed in Alzheimer's disease (AD) have been suggested to begin at the entorhinal cortex and hippocampus and then to propagate in a stereotypical fashion. Using diffusion-weighted imaging, we test whether disruption of structural connectivity in AD is centered on these "epicenters of disease". **Methods:** Fifteen healthy controls, 14 amnestic mild cognitive impairment (aMCI), 13 mild, and 15 moderate patients with AD were enrolled. The percentages of affected connections directly linking to the epicenter (named first ring) and to nodes with topological distance 2 from the epicenter (named second ring) were calculated. **Results:** For the group of aMCI patients, just 5.3% of the first ring (n.s.) and 2.9% of the second ring (n.s.) connections were affected. However, for mild AD there was disruption involving 20% of the first ring ($P < 0.0001$) and 10.3% of the second ring ($P < 0.0001$) connections. In the moderate AD group, a stronger effect was observed, with 38.0% of the first ring ($P < 0.0001$) connections and 17.9% of the second ring ($P < 0.0001$) connections affected. **Conclusion:** Our results favor an epicentral disruption of structural connectivity in aMCI and AD around entorhinal and hippocampal regions, consistent with the transneuronal spread hypothesis.

The first two authors contributed equally to this work.

doi: 10.1111/cns.12397

Introduction

Alzheimer's disease (AD) is a progressive neurodegenerative disorder, known as the most common form of dementia [1]. The two neuropathological hallmarks of AD are neurofibrillary tangles (NFTs), related to intraneuronal formation of hyperphosphorylated tau protein, and neuritic plaques (NPs) composed of extracellular deposits of amyloid beta (Aβ) protein [2–4]. Pathology studies have shown that AD-related neuropathological changes, especially NFTs, begin at specific sites of the human brain and then propagate from affected to unaffected areas in a systematic and stereotypical fashion [2–6]. Indeed, the first brain regions affected by NFTs are the transentorhinal and the entorhinal cortex (EC), followed by the hippocampus (HIP) [2–6]. It is until a later phase of the disorder that the neocortex and especially the associative areas are thought to become involved in the disease process related to NFTs [2–6]. Structural MRI studies have shown supporting evidence that EC and HIP are the first affected brain regions in subjects with mild cognitive impairment (MCI) and AD, and, furthermore, that the atrophy pattern in EC and HIP can predict the conversion from MCI to AD [7,8].

There is a growing body of research showing that network analyses contribute greatly to the understanding of brain dysfunction [9]. Abnormal structural connectivity has indeed been revealed in several psychiatric [10] and neurological disorders, including AD [11]. Four major models of network-based neurodegeneration spread have been proposed. In the ''nodal stress'' model, regions with high neural activity are damaged due to a ''wear and tear'' mechanism [12–14]. The ''trophic failure'' model assumes connectivity impairment to cause failure of inter-

nodal trophic factor, promoting neurodegeneration [15,16]. In the "shared vulnerability'' model, a common disease-specific gene or protein expression underlies the susceptibility of specific regions of a network [17]. Last, the ''transneuronal spread'' model is based on the hypothesis that toxic agents propagate along brain connections with a prion-like behavior [18,19]. Recently, Zhou and colleagues used graph theoretical analysis to investigate how intrinsic functional connectivity in health predicts the brain's vulnerability to neurodegeneration [17]. Their findings suggested the transneuronal model as the most likely to underlie the changes observed in neurodegenerative diseases including AD [17].

Here, using graph theoretical analysis of diffusion-weighted imaging (DWI) data, we tested the hypothesis that structural connectivity of AD and amnestic mild cognitive impairment (aMCI) patients might be explained by the transneuronal spread model, focusing specifically on the topological distance of nodal connectivity from the EC/HIP, *a priori* selected as a potential disease epicenter. Disease effects of reduced structural connectivity were expected to be stronger at shorter topological distance from the EC/HIP epicenter. Correlations between connectivity measures and Mini Mental State Examination (MMSE) scores were assessed, to test a possible relationship between neurodegenerative effects of global, EC, and HIP connectivity disruption and cognitive performance in patients.

Materials and Methods

Subjects and Clinical Evaluation

The study was approved by the local ethical committee and was conducted in accordance with the Declaration of Helsinki. All subjects or caregivers provided their written informed consent to use their anonymized data for research purposes.

In total, 57 subjects, of which 15 healthy controls (HC), 14 aMCI, 13 mild AD, and 15 moderate AD, were included in this study. Demographics and clinical characteristics are listed in Table 1. All subjects were recruited from the outpatient clinic of Neurology Unit at Università Campus Bio-Medico di Roma (Italy). Each subject underwent medical, neurological, cognitive, and laboratory screening together with an MRI scan of the brain, reviewed by two independent and experienced neuroradiologists to rule out structural abnormalities. A detailed description of the administered neuropsychological test battery is provided in the Data S1.

The diagnosis of AD or aMCI was made by two independent, experienced neurologists according to the criteria of the National Institute of Neurological and Communicative Disorders and Stroke and the Alzheimer's Disease and Related Disorders Association (NINCDS-ADRDA) [20] and to the criteria of Petersen [21], respectively. Patients with AD were further classified into two groups based on the corrected MMSE scores (adjusted for age and education), being mild AD (22–27), and moderate AD (10–20) [22,23]. Severity differences were confirmed using the Clinical Dementia Rating (CDR) scale [24,25].

For aMCI patients exclusion criteria included mild AD, concomitant dementia, reversible dementias, fluctuations in cognitive performance, mixed dementias, concomitant extra-pyramidal symptoms, depression with Geriatric Depression Scale (GDS) scores >13, other psychiatric diseases, epilepsy, drug or alcohol addiction, use of psychoactive drugs, systemic diseases, traumatic brain injuries, and use of cholinergic drugs. For patients with AD, exclusion criteria included frontotemporal dementia [26], vascular dementia [27], extra-pyramidal syndromes, reversible dementias (including pseudodementia of depression and normotensive hydrocephalus) and Lewy body dementia [28]. Healthy subjects were recruited among non-consanguineous relatives of the patients and through advertisements. All healthy subjects met the criteria of having a GDS score <13 and a MMSE score ≥27 and did not have a history of neurological or psychiatric diseases, chronic systemic illnesses or use of psychoactive drugs. In total, this resulted in the inclusion of 57 subjects divided into 4 groups: aMCI (14 patients), mild AD (13 patients), moderate AD (15 patients), and the healthy control group (15 subjects).

Imaging Acquisition

Images were acquired using a 1.5 Tesla MRI system (Avanto B13, Siemens, Erlangen, Germany), configured with a 12-element designed Head Matrix Coil. The imaging protocol included the following: structural T1-weighted MPRAGE (Magnetization Prepared Rapid Acquisition with Gradient Echo) sequences (TR

Table 1 Demographic and clinical features of the diagnostic groups

	HC (N = 15)	aMCI (N = 14)	Mild AD (N = 13)	Moderate AD (N = 15)	χ^2 or F	*P* value
Gender (men, women)	7, 8	10, 4	8, 5	8, 7	0.57	n.s.
Age years (SD)	73.1 (6.1)	74.4 (5.9)	74.5 (9.7)	74.9 (4.8)	0.21	n.s.
Range	61–84	63–85	58–89	63–82		
Education years (SD)	6.9 (3.2)	8.8 (4.3)	10.2 (4.7)	9.0 (4.9)	1.15	n.s.
Range	5–15	4–18	5–17	4–18		
MMSE raw score (SD)	28.6 (1.1)	26.9 (2.2)	23.6 (1.7)	17.9 (3.1)	61.9	$<10^{-7}$
Range	27–30	23–30	22–28	13–23		
Corrected score (SD)	28.2 (1.1)	26.3 (2.5)	22.5 (1.1)	17.2 (2.5)	83.3	$<10^{-7}$
Range	26.7–30.0	22.3–30.0	21.0–24.4	12.9–21.3		
CDR	0	0.5	1	2		

HC, healthy controls; aMCI, amnestic mild cognitive impairment; AD, Alzheimer's disease; MMSE, Mini-Mental-State Examination; CDR, Clinical Dementia Rating; SD, standard deviation.

2400 ms, TE 3.61 ms, TI 1000 ms, FOV read 240 mm, FOV phase 100.0%, flip angle 8°, slice thickness 1.20 mm, averages 1, slice for slab 160, slab 1, bandwidth 180 Hz/Px) and T2-/PD-weighted TSE (Turbo Spin Echo) sequences (TR 3000 ms, TE1 12 ms, TE2 92 ms, FOV read 240 mm, FOV phase 89.1%, flip angle 150°, slice thickness 3 mm, averages 1, slices 48, bandwidth 163 Hz/Px), according to the Italian Alzheimer Disease Neuroimaging Initiative (ADNI) harmonization protocol. Diffusion-weighted images (DWI) were acquired with a weighting 1000 mm^2/s and with gradients applied in 12 different directions, together with a b0 scan (slice group 1, slices 38, dist factor 30%, phase enc. dir. A ≫ P, phase oversampling 0%, FOV read 250 mm, FOV phase 100%, slice thickness 3 mm, TR 7600 ms, TE 103 ms, concatenations 1, coil elements BO1.2.SP4.5). Four complete sets (each of 12 directions) were acquired, providing a total of four b0 and 48 diffusion-weighted volumes.

Construction of Structural Brain Networks

Individual structural brain networks were reconstructed on the basis of a parcellation of the brain into 83 distinct brain regions combined with white matter fibers resulting from tractography (see Data S1 for details including T1 and DWI preprocessing and tractography). The networks, mathematically described as a graph consisting of a collection of nodes (brain regions) and a collection of edges between nodes (white matter tracts), were represented by 83 × 83 structural connectivity matrices storing information regarding the existence, absence, and weight of a connection between node i and j in cell $c(i,j)$. Fractional anisotropy (FA) was chosen as a measure of microstructural fiber directionality and the number of streamlines (NOS) as a measure to quantify the absolute number of connection fibers. Streamline density (NOS divided by the mean volume of the two interconnected nodes [29,30]) was added in an attempt to account for potential effects of cortical atrophy on NOS metrics.

Global Connectivity Strength

The Jonckheere–Terpstra test was used to assess whether average global connectivity strength, that is, the sum of all connection strengths per subject, decreased from the HC group to the aMCI, mild AD, and moderate AD groups, effectively testing for potential ordering of three or more population medians. Global connectivity strength levels were controlled for age, gender, and education effects using a linear regression model.

Connectivity Ring Analysis

To test whether disease progression from aMCI to mild and moderate AD could be reflected by structural damage to the epicenter, the percentage of connections to the epicenter that were affected was computed for all three groups of patients and was compared to the control population (Figure 1). First, individual connectivity matrices were masked to keep those connections that were present in at least 50% of the healthy control subjects [31,32]. Second, two rings of nodes were defined. A first ring of nodes directly linked by one connection to either one of the epicenter nodes, and a second ring of nodes at topological distance two from the epicenter [33]. Third, the strengths of connections between the epicenter and the first ring and between first and second ring were compared in each of the three groups of patients with those observed in the control population. In each patient group separately, connections that showed a lower average strength compared to the HC group (t-test, P-value <0.05) were labeled as "affected" following an approach similar as defined by Network Based Statistics (NBS) [34]. As for the global analysis, connection strengths were controlled for age, gender, and education effects using a linear regression model. Next, the percentage of affected connections was computed for the two rings in each patient group. This procedure was carried out for both hemispheres separately, and percentages of affected connections were subsequently averaged. Fourth, significance of the findings was assessed by means of permutation testing. For each of the three patient groups, the analysis was repeated for 10,000 random permutations of group assignments (i.e., HC or patient) to obtain a distribution of results under the null hypothesis.

Examining Specificity of the *a priori* Selected Epicenter

In addition, to assess the merit of selecting the EC and HIP as the epicenter, the analysis described above was carried out for all possible epicenters consisting of two homologous node pairs ($41 \times 40/2 = 820$) according to the used gray matter parcellation. For each of the three patient groups, the share of all possible epicenters yielding higher percentages of affected connections than the original EC and HIP epicenter in both the first and second ring denoted the P-value.

Relationship between Structural Connectivity and MMSE

To assess a potential link between global structural connectivity and cognition, for each patient the strengths of all connections present in the connectivity matrices were summed and examined for a correlation with corrected MMSE scores. To analyze the correlation between MMSE scores and structural connectivity of the epicenter regions specifically, strength values were summed of all connections linking to the HIP or EC regions. Global and epicenter connectivity strengths were controlled for age, gender, and education effects using a linear regression model. Pearson's correlation coefficient was used to assess correlations between connectivity strengths and MMSE scores.

Results

Demographic and Clinical Features

When the global cognitive status was assessed by means of MMSE, the four groups (HC, aMCI, mild AD, and moderate AD) differed significantly ($F_{3,53} = 61.9$; $P < 0.0001$). *Post hoc* comparisons (Fisher LSD test) showed that all groups differed significantly between each other ($P < 0.0001$). A similar effect was observed for corrected MMSE scores ($F_{3,53} = 83.3$; $P < 0.0001$). No significant difference among groups was observed in age ($F_{3,53} = 0.21$; p = n.s.) and education level ($F_{3,53} = 1.15$; p = n.s.).

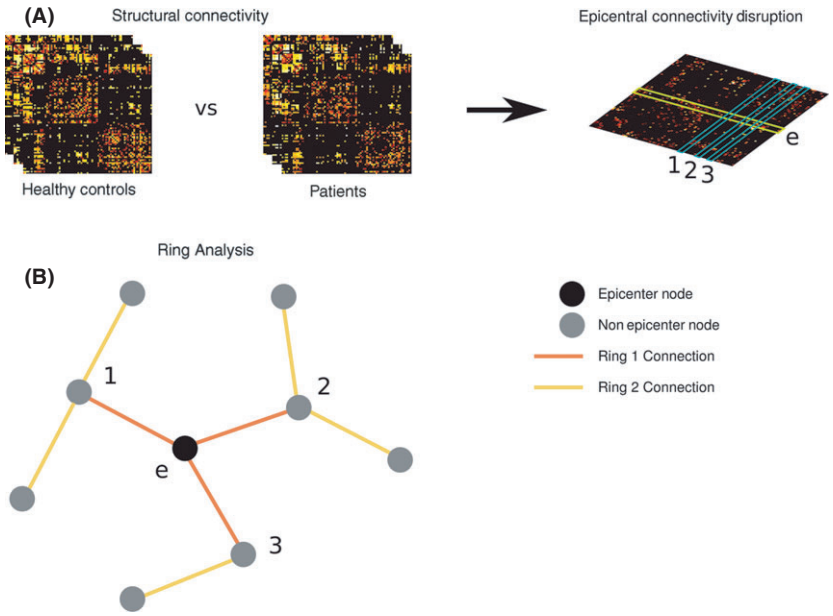

Figure 1 (**A**) Structural connectivity analysis of patients compared with healthy controls using matrices. (**B**) Two classes of connections were defined relative to the epicenter, referred to as first and second ring connections. First ring connections are those directly linking to the epicenter (orange lines in (**B**)), second ring connections are those with topological distance 2 from the epicenter (yellow lines in (**B**)).

Global Connectivity Strength

Two-sample *t*-tests on NOS global strengths of each patient group versus the HC group showed no significant global effects for aMCI (n.s.; $P = 0.88$) and mild AD (n.s.; $P = 0.17$), while a significant global effect was observed in moderate AD ($P = 0.03$). These findings suggest that only in moderate AD the connectivity disruption is widespread to an extent that enables detection of a global effect. Similar results were found using FA: aMCI (n.s.; $P = 0.85$), mild AD (n.s.; $P = 0.43$), and moderate AD ($P = 0.05$) as compared to controls. No significant global effect was observed for any of the groups using streamline density (aMCI n.s.; $P = 0.45$; mild AD n.s.; $P = 0.98$; moderate AD n.s.; $P = 0.58$).

Additional nonparametric Jonckheere–Terpstra testing revealed a significant group ordering effect for NOS ($P < 0.01$) and FA ($P = 0.02$), indicative of a progressive reduction of structural connectivity across patients groups as compared to controls (Figure 2). No significant group ordering effect was found using streamline density (n.s.; $P = 0.32$).

Connectivity Ring Analysis

To investigate whether pathways linking to nodes with lower topological distance to the selected EC/HIP were characterized by greater structural damage, the percentage of affected connections was calculated for connections directly linking to the EC/HIP and connections between first and second ring nodes. The total number of connections and nodes belonging to the first and second ring is listed in Table 2.

Number of Streamlines

Connectivity ring analysis based on NOS yielded a total of 15, 50, and 94 affected connections of which 13%, 16%, and 16% were first ring connections, and 60%, 62%, and 58% were second ring connections, in the aMCI, mild, and moderate AD groups, respectively.

Among all connections of the first ring, 5.3% were found to be affected (i.e., *t*-test, $P < 0.05$) (n.s.; $P = 0.11$) for the aMCI group, together with just 2.9% in the second ring (n.s.; $P = 0.18$). For mild AD, 20.0% of connections in the first ring ($P < 0.0001$) and 10.3% in the second ring were found affected ($P < 0.0001$), and more severely, for the moderate AD group 38.0% of connections were found affected in the first ring ($P < 0.0001$) and 17.9% in the second ring ($P < 0.0001$) (Figure 3). Moreover, controlling for cortical atrophy effects, streamline density analysis revealed supportive effects for reduced EC/HIP connectivity. Using streamline density, a total of 31, 38, and 68 affected connections of which 8%, 13%, and 16% were first ring connections, and 54%, 68%, and 56% were second ring connections, in the aMCI, mild, and moderate AD groups, respectively.

In the aMCI group, 2.6% of connections in the first ring (n.s.; $P = 0.34$) were found affected, with 2.3% in the second ring (n.s.; $P = 0.32$). For mild AD, 12.7% of connections in the first ring ($P = 0.0038$) and 8.6% in the second ring ($P < 0.0001$) were affected, while in the moderate AD, 28.2% of first ring connections ($P < 0.0001$) and 12.5% second ring connections ($P < 0.0001$) were found to be affected.

Fractional Anisotropy

Examining FA, a total of 30, 53, and 77 affected connections of which 3%, 13%, and 14% were first ring connections, and 80%, 72%, and 60% were second ring connections, in the aMCI, mild, and moderate AD groups, respectively. For the aMCI group, 2.6% connections in the first ring (n.s.; $P = 0.43$) and 7.9% in the second ring ($P = 0.0003$) were affected; for mild AD, 17.4% of connections in the first ring ($P = 0.0003$) and 12.3% in the second ring ($P < 0.0001$) were found affected; for

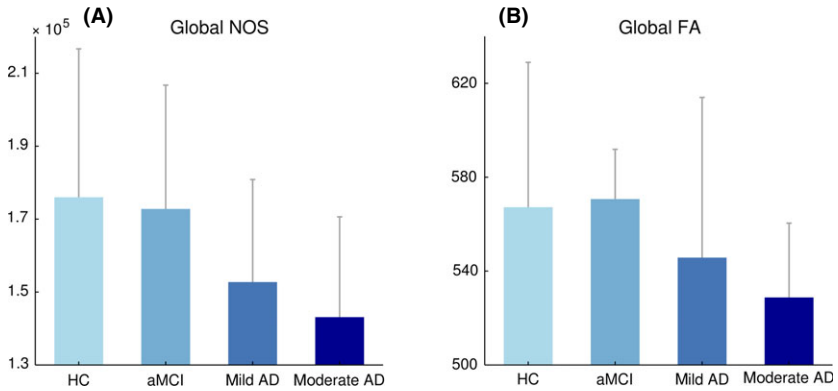

Figure 2 Global effect evaluated as the sum of all connection strengths per subject for NOS (**A**) and FA (**B**). A significant group ordering effect for global NOS (**A**) as well as for FA (**B**), showing progressive reduction of global structural connectivity across groups. Error bars represent standard deviations.

Table 2 Regions and total number of connections of each ring centered on the epicenter

	LH Ring 1	RH Ring 1	LH Ring 2	RH Ring 2
Number of connections	21	19	167	142
Node names	Thalamus	Thalamus	Accumbens area	Accumbens area
	Caudate	Caudate	Caudal anterior cingulate	Caudal anterior cingulate
	Putamen	Putamen		
	Pallidum	Pallidum	Caudal middle frontal	Cuneus
	Amygdala	Amygdala	Cuneus	Inferior parietal
	Fusiform	Fusiform	Inferior parietal	Lateral occipital
	Inferior temporal	Inferior temporal	Lateral occipital	Lateral orbitofrontal
	Isthmus cingulate	Isthmus cingulate	Lateral orbitofrontal	Medial orbitofrontal
	Lingual	Lingual	Medial orbitofrontal	Middle temporal
	Parahippocampal	Parahippocampal	Middle temporal	Paracentral
	Pericalcarine	Precuneus	Paracentral	Pars opercularis
	Precuneus	Superior parietal	Pars opercularis	Pars orbitalis
	Superior frontal	Temporal pole	Pars orbitalis	Pars triangularis
	Superior parietal		Pars triangularis	Pericalcarine
	Temporal pole		Postcentral	Postcentral
	Insula		Posterior banks of superior temporal	Posterior banks of superior temporal
			Posterior cingulate	Posterior cingulate
			Precentral	Precentral
			Rostral anterior cingulate	Rostral anterior cingulate
			Rostral middle frontal	Rostral middle frontal
			Superior temporal	Superior frontal
			Supramarginal	Superior temporal
			Frontal pole	Supramarginal
			Transverse temporal	Frontal pole
			Brain Stem	Transverse temporal
				Insula
				Brain Stem

LH, Left Hemisphere; RH, Right Hemisphere.

moderate AD, 27.9% of connections in the first ring ($P = 0.0001$) and 14.9% in the second ring ($P < 0.0001$) were found to be affected.

Significant overlap was observed between the affected connections in the three patient groups for all investigated diffusion measures (NOS, streamline density, and FA), in support of the *a priori* selected EC/HIP epicenter, see Data S1.

Examining Specificity of the *a priori* Selected Epicenter

The reported proportions of affected connections, based on NOS and FA, were found to be specific for our epicenter selection consisting of the EC and HIP nodes ($P < 0.02$). The analysis of streamline density confirmed a specific effect for the selected epicenter in

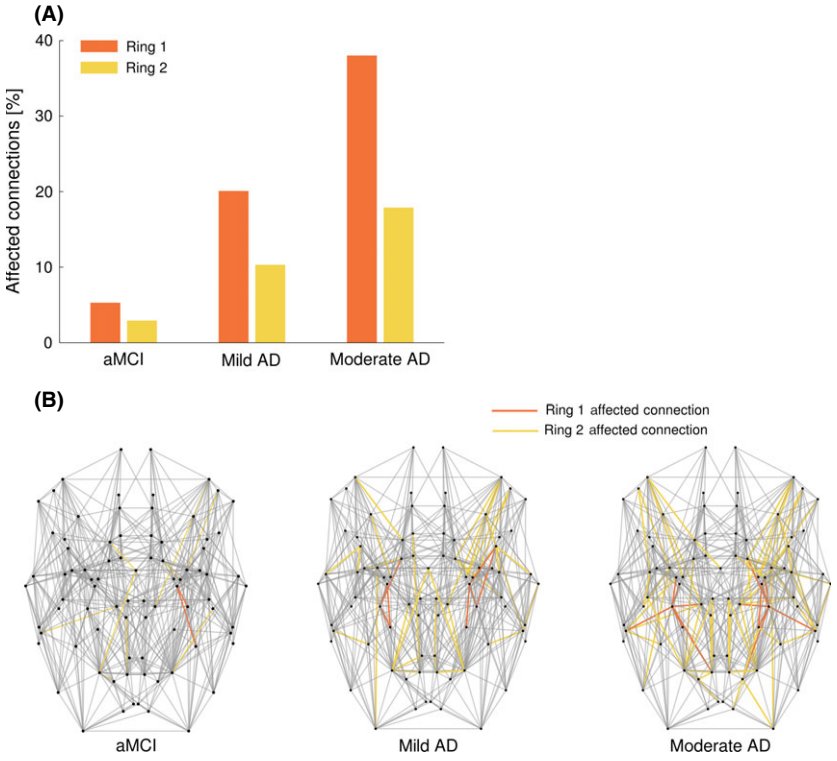

Figure 3 (**A**) Bar plot showing the percentage of affected connections for the first and second ring in each group of patients. (**B**) NOS-weighted brain network for each group of patients showing the affected connections colored in orange for the first ring and in yellow for the second ring. The locations of homologous nodes, based on anatomy, have been symmetrized. For all groups, a greater percentage of connections were affected in the first ring as compared to the second (**A**) and a progressive increase of affected connections was observed across groups (**B**).

terms of affected connections in both patient with AD groups ($P < 0.01$), but not in the aMCI patients (n.s., $P = 0.13$). Less than 2% (NOS and FA) of all other possible combinations of nodes (n = 41 × 40/2 = 820 unique combinations of two nodes out of the 41 that make up one hemisphere) showed an equal or stronger effect than the EC and HIP combination, confirming the appropriateness of the *a priori* selected epicenter. Importantly, no node combination scored higher in both rings and in all three patient groups than our chosen EC/HIP epicenter. Furthermore, the majority of possible alternative epicenters overlapped with the original EC/HIP epicenter, containing either the EC or HIP, or included the parahippocampal gyrus which is directly connected to the HIP [35] and known to be involved in AD [36]. Apart from the EC, HIP, or parahippocampal gyrus, the cingulate and middle frontal regions show strong involvement in patients with aMCI and AD, consistent with the literature [37,38].

Relationship between Structural Connectivity and MMSE

A significant correlation between corrected MMSE scores and global connectivity strength based on NOS (r = 0.36; $P = 0.02$) as well as global connectivity strength based on FA (r = 0.34; $P = 0.03$) was observed (Figure 4A–B). For left and right HIP together, we found significant correlations with MMSE for both NOS (r = 0.43; $P < 0.01$), FA (r = 0.47; $P < 0.01$) and streamline density (r = 0.34; $P = 0.03$, correcting for regional volume effects) (Figure 4C–D). No significant correlation was observed between MMSE and structural connectivity strength (FA, NOS, and streamline density) of the left and right EC, nor between MMSE and global connectivity strength based on streamline density (r = 0.02; $P = 0.90$). Also, no significant correlations were observed between MMSE score and structural connectivity strength (FA, NOS, and streamline density) within any group taken separately.

Conclusion

Our findings demonstrate reduced structural connectivity in AD and aMCI patients with respect to controls, with a topological pattern that it is centered on the EC and HIP. White matter involvement surrounding the epicenter regions entorhinal cortex and hippocampus was found to increase with worsening of disease status from aMCI to moderate AD. In this study, graph theoretical analysis was used to assess the structural connectivity changes in AD and aMCI and our findings support the transneuronal model of disease spread.

Zhou and colleagues recently investigated four models of neurodegeneration ("nodal stress," "trophic failure," "shared vulnerability," and "transneuronal spread") and defined, for each of five different neurodegenerative disorders, critical "epicenters" as the regions whose seed-based intrinsic functional connectivity map in healthy subjects best match the disease-related atrophy pattern [17]. They reported the vulnerability of a node to be best predicted by its greater total connectional flow and by a shorter functional path to the disease-related epicenters. Furthermore, they put forward the transneuronal spread as the best model to fit processes of neurodegeneration [17], a conclusion consistent with our currently presented findings of epicentral structural connectivity disruptions around the EC/HIP.

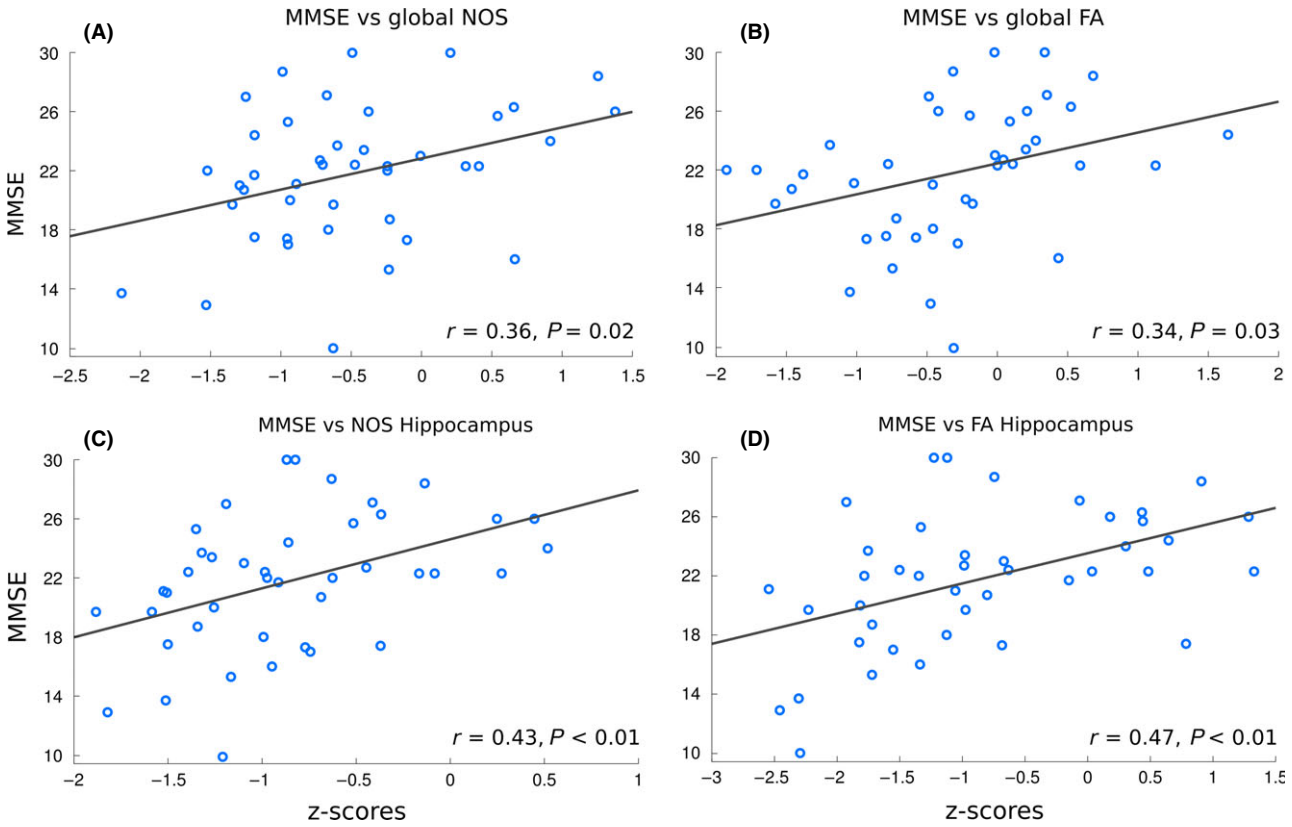

Figure 4 Scatter plots indicating significant correlations between cognitive status (i.e., MMSE) and structural connectivity metrics: global NOS (**A**), global FA (**B**), hippocampus NOS (**C**), and hippocampus FA (**D**).

The EC and HIP are two brain regions located in the medial temporal lobes. Spatially, EC and HIP are regions located close to each other. EC, indeed, is known to merge with structures belonging either to the hippocampal formation or the parahippocampal region on its medial side and with the perirhinal and the parahippocampal cortex on its lateral and posterior side [39]. As it is known from early anatomical studies, EC and HIP are strongly inter connected, thus suggesting a common physiological significance of the two structures [39]. Moreover, HIP is noted to be involved in declarative memory processes [40] and the EC is believed to be involved in memory functions [39]. Although its specific functional contributions remain to be clearly determined, EC is considered to be the nodal point of connection between the hippocampal formation and the multimodal association areas [39]. The above anatomical notions support the biological rationale of this study to focus on a disease epicenter based on EC and HIP, two brain regions closely linked and related to each other.

From a neuropathological point of view, intracellular neurofibrillary tangles (NFTs) are first found in the EC, then in the HIP and later on in other regions [2–6]. As the selected epicenter is noted to be more involved in tau protein than beta accumulation, especially in early stages of AD [41,42], where a random distribution of cortical amyloid beta deposits has been observed, the results of our study possibly relate to the effects of tau protein. The distribution of NFTs in the human cerebral cortex is noted to closely match, on a laminar and regional basis, that of pyramidal neurons enabling cortico-cortical connections between and within hemispheres [43–46], observations consistent with a latent interplay between cytoarchitectural features of cortical regions and their global cortico-cortical connectivity fingerprint [47]. Furthermore, neuritic plaques (NPs) and NFTs have been observed to be localized in the same cortical layers reached by the terminal axons of the perforant pathways both within the hippocampal formation and the dentate gyrus [6,48]. Thus, a connectivity-based approach, as used in our study, provides more insight into the widespread involvement of brain regions in AD and, selecting the HIP and EC as the epicenter of connectivity disruption in AD allows for exploring the association of neuropathological changes with neurodegenerative processes.

Our current study hypothesized that AD pathology may propagate stepwise along white matter pathways and that the clinical expression of AD could be supported by selective vulnerability of subtypes of pyramidal neurons and consequent loss of cortico-cortical connections, resulting in a so-called disconnection syndrome [3–6,23]. Results indicate that the progressive structural connectivity impairment (aMCI <mild AD <moderate AD) of pathways linking to nodes with lower topological distance to the epicenter begins in circumscribed sites and then gradually involves connection-wise neighboring regions. Indeed, the connectivity ring analysis showed the same pattern of reduction for all metrics used (FA, NOS, streamline density) as disease severity increased. Although it may be argued that the percentage of affected tracts

may be influenced by the different number of connections between ring 1 and ring 2 (i.e., ring 1 < ring 2), the progressive increase of affected connections in the first ring with the severity of the disease supports the notion that shorter topological distance from the epicenter of disease is associated with higher percentage of affected connections. The global connectivity analysis showed a significant reduction of FA and NOS only for the moderate AD group, suggesting that the connectivity ring analysis centered on the HIP/EC is more sensitive than a global approach to detect early connectivity changes associated to aMCI and AD.

The major aim of the study was to test a transneuronal spread model by examining potential epicentral structural connectivity disruptions. However, in this context, it is critical to specifically assess whether the total connectional flow ("nodal stress" model) may better explain the observed effects. Thus, to examine the "nodal stress" hypothesis, in a *post hoc* analysis, the connectivity ring analysis was performed for different selections of hub regions (see Data S1) that have been demonstrated to show strong connectional flow [12,29,49] and that have been suggested to form an anatomical substrate for integration among functional networks [30]. Taking these "hub nodes" as potential disease epicenters did not result in differences between connectivity effects in the first and second ring (Figure S1) as was observed for the EC/HIP epicenter (Figure 3), suggesting that the total connectional flow did not affect our results and that the ''wear and tear'' mechanism is less likely to explain observed patterns of structural connectivity disruptions.

Global NOS and FA measures significantly correlated with MMSE, revealing a relationship between the level of dysconnectivity and cognitive status in patients. The regions belonging to the epicenter were also explored separately: Significant correlations between HIP structural connectivity and MMSE were observed, while no significant correlations were found with EC; these results suggest a significant impact of the HIP structural connectivity on the patient's cognitive status.

It is important to note that our current study does not include longitudinal data. Such data would be of great interest in order to strengthen findings and to confirm a spatiotemporal connection-driven disease spread in AD. Moreover, although our results are consistent with transneuronal disease spread, they do not allow for a direct demonstration of transneuronal transfer of potential toxic agents. In addition, on a more technical note, a single-tensor deterministic approach was used in our connectome reconstruction (as the data described only 12 diffusion directions), which might yield inaccurate fiber reconstructions in voxels of crossing fibers [50,51]. Future studies examining probabilistic fiber tracking and/or multi-tensor approaches in AD structural connectivity would be of particular interest to elucidate the impact of crossing fibers voxels on our results. Using different imaging modalities, for example, functional MRI and FDG-PET, other regions, most prominently in the default mode network including the posterior cingulate gyrus and the precuneus, have been shown to be early involved in MCI and AD [52–55]. These diverging functional and structural findings call for future integrative studies providing more insight into the structure–function relationship in AD.

The results of this study support an epicentral disruption of structural connectivity in aMCI and AD, consistent with the effects of a potential transneuronal spread of disease. EC and HIP together represent a good target to be considered the epicenter of anatomical connectivity impairment in aMCI and AD.

Acknowledgments

We are thankful to Federica Scrascia, MD for her assistance in the recruitment of the subjects enrolled in this study. MPvdH was supported by a VENI grant (#451-12-001) of the Netherlands Organization for Scientific Research (NWO) and by a Fellowship of the Brain Center Rudolf Magnus.

Conflict of Interest

The authors declare no conflicts of interest.

References

1. Kukull WA, Bowen JD. Dementia epidemiology. *Med Clin North Am* 2002;**86**:573–590.
2. Braak H, Braak E. Neuropathological stageing of Alzheimer-related changes. *Acta Neuropathol* 1991;**82**:239–259.
3. Braak H, Del Tredici K. Alzheimer's pathogenesis: Is there neuron-to-neuron propagation? *Acta Neuropathol* 2011;**121**:589–595.
4. Reid AT, Evans AC. Structural networks in Alzheimer's disease. *Eur Neuropsychopharmacol* 2013;**23**:63–77.
5. Delbeuck X, Van Der LM, Collette F. Alzheimer's disease as a disconnection syndrome? *Neuropsychol Rev* 2003;**13**:79–92.
6. De Lacoste MC, White CL 3rd. The role of cortical connectivity in Alzheimer's disease pathogenesis: A review and model system. *Neurobiol Aging* 1993;**14**:1–16.
7. Devanand DP, Pradhaban G, Liu X, et al. Hippocampal and entorhinal atrophy in mild cognitive impairment: Prediction of Alzheimer disease. *Neurology* 2007;**68**:828–836.
8. Pennanen C, Kivipelto M, Tuomainen S, et al. Hippocampus and entorhinal cortex in mild cognitive impairment and early AD. *Neurobiol Aging* 2004;**25**:303–310.
9. Tijms BM, Wink AM, de Haan W, et al. Alzheimer's disease: Connecting findings from graph theoretical studies of brain networks. *Neurobiol Aging* 2013;**34**:2023–2036.
10. Van den Heuvel MP, Mandl RCW, Stam CJ, Kahn RS, Hulshoff Pol HE. Aberrant frontal and temporal complex network structure in schizophrenia: A graph theoretical analysis. *J Neurosci* 2010;**30**:15915–15926.
11. Lo C-Y, Wang P-N, Chou K-H, Wang J, He Y, Lin C-P. Diffusion tensor tractography reveals abnormal topological organization in structural cortical networks in Alzheimer's disease. *J Neurosci* 2010;**30**:16876–16885.
12. Buckner RL, Sepulcre J, Talukdar T, et al. Cortical hubs revealed by intrinsic functional connectivity: Mapping, assessment of stability, and relation to Alzheimer's disease. *J Neurosci* 2009;**29**:1860–1873.
13. Saxena S, Caroni P. Selective neuronal vulnerability in neurodegenerative diseases: From stressor thresholds to degeneration. *Neuron* 2011;**71**:35–48.
14. de Haan W, Mott K, van Straaten E, Scheltens P, Stam CJ. Activity dependent degeneration explains hub vulnerability in Alzheimer's Disease. *PLoS Comput Biol* 2012;**8**:e1002582.
15. Appel SH. A unifying hypothesis for the cause of amyotrophic lateral sclerosis, parkinsonism, and Alzheimer disease. *Ann Neurol* 1981;**10**:499–505.
16. Salehi A, Delcroix J-D, Belichenko PV, et al. Increased App expression in a mouse model of Down's syndrome disrupts NGF transport and causes cholinergic neuron degeneration. *Neuron* 2006;**51**:29–42.
17. Zhou J, Gennatas ED, Kramer JH, Miller BL, Seeley WW. Predicting regional neurodegeneration from the healthy brain functional connectome. *Neuron* 2012;**73**:1216–1227.
18. Frost B, Diamond MI. Prion-like mechanisms in neurodegenerative diseases. *Nat Rev Neurosci* 2010;**11**:155–159.
19. Lee S-J, Desplats P, Sigurdson C, Tsigelny I, Masliah E. Cell-to-cell transmission of non-prion protein aggregates. *Nat Rev Neurol* 2010;**6**:702–706.
20. McKhann GM, Knopman DS, Chertkow H, et al. The diagnosis of dementia due to Alzheimer's disease: Recommendations from the National Institute on Aging-Alzheimer's Association workgroups on diagnostic guidelines for Alzheimer's disease. *Alzheimers Dement* 2011;**7**:263–269.

21. Petersen RC, Doody R, Kurz A, et al. Current concepts in mild cognitive impairment. *Arch Neurol* 2001;**58**:1985–1992.
22. Folstein MF, Folstein SE, McHugh PR. "Mini-mental state". A practical method for grading the cognitive state of patients for the clinician. *J Psychiatr Res* 1975;**12**:189–198.
23. Scrascia F, Curcio G, Ursini F, et al. Relationship among diffusion tensor imaging, EEG activity, and cognitive status in mild cognitive impairment and Alzheimer's Disease patients. *J Alzheimers Dis* 2013;**38**:939–950.
24. Hughes CP, Berg L, Danziger WL, Coben LA, Martin RL. A new clinical scale for the staging of dementia. *Br J Psychiatry* 1982;**140**:566–572.
25. Morris JC. The clinical dementia rating (CDR): Current version and scoring rules. *Neurology* 1993;**43**:2412–2414.
26. Englund B, Brun A, Gustafson L, et al. Clinical and neuropathological criteria for frontotemporal dementia. *J Neurol Neurosurg Psychiatry* 1994;**57**:416–418.
27. Román GC, Tatemichi TK, Erkinjuntti T, et al. Vascular dementia: Diagnostic criteria for research studies. Report of the NINDS-AIREN International Workshop. *Neurology* 1993;**43**:250–260.
28. McKeith I, O'Brien J, Ballard C. Diagnosing dementia with Lewy bodies. *Lancet* 1999;**354**:1227–1228.
29. Hagmann P, Cammoun L, Gigandet X, et al. Mapping the structural core of human cerebral cortex. *PLoS Biol* 2008;**6**:e159.
30. Van den Heuvel MP, Sporns O. Rich-Club organization of the human connectome. *J Neurosci* 2011;**31**:15775–15786.
31. De Reus MA, van den Heuvel MP. Estimating false positives and negatives in brain networks. *NeuroImage* 2013;**70**:402–409.
32. Verstraete E, Veldink JH, van den Berg LH, Van den Heuvel MP. Structural brain network imaging shows expanding disconnection of the motor system in amyotrophic lateral sclerosis. *Hum Brain Mapp* 2014;**35**:1351–1361.
33. Schmidt R, Verstraete E, de Reus MA, Veldink JH, van den Berg LH, van den Heuvel MP. Correlation between structural and functional connectivity impairment in amyotrophic lateral sclerosis. *Hum Brain Mapp* 2014;**35**:4386–4395.
34. Zalesky A, Fornito A, Bullmore ET. Network-based statistic: Identifying differences in brain networks. *NeuroImage* 2010;**53**:1197–1207.
35. Powell HWR, Guye M, Parker GJM, et al. Noninvasive in vivo demonstration of the connections of the human parahippocampal gyrus. *NeuroImage* 2004;**22**:740–747.
36. Van Hoesen GW, Augustinack JC, Dierking J, Redman SJ, Thangavel R. The parahippocampal gyrus in Alzheimer's disease: Clinical and preclinical neuroanatomical correlates. *Ann N Y Acad Sci* 2000;**911**:254–274.
37. Zhang Y, Schuff N, Jahng GH, et al. Diffusion tensor imaging of cingulum fibers in midl cognitive impairment and Alzheimer disease. *Neurology* 2007;**68**:13–19.
38. Davatzikos C, Fan Y, Wu X, Shen D, Resnick SM. Detection of prodromal Alzheimer's disease via pattern classification of magnetic resonance imaging. *Neurobiol Aging* 2008;**29**:514–523.
39. Canto CB, Wouterlood FG, Witter MP. What does the anatomical organization of the entorhinal cortex tell us? *Neural Plast* 2008;**2008**:381243.
40. Mallio CA, Assenza G, Occhicone F, Errante Y, Zobel BB, Quattrocchi CC. Transient global amnesia and hippocampal foci of restricted diffusion. *BMJ Case Rep* 2013;**10**:2013.
41. Hatashita S, Yamasaki H. Diagnosed mild cognitive impairment due to Alzheimer's Disease with PET biomarkers of beta amyloid and neuronal dysfunction. *PLoS ONE* 2013;**8**:e66877.
42. Prescott JW, Guidon A, Doraiswamy PM, Choudhury KR, Liu C, Petrella J. The alzheimer structural connectome: Changes in cortical network topology with increased amyloid plaque burden. *Radiology* 2014;**273**:175–184.
43. Gómez-Isla T, Price J. Profound loss of layer II entorhinal cortex neurons occurs in very mild Alzheimer's disease. *J Neurosci* 1996;**16**:4491–4500.
44. Lewis DA, Campbell MJ, Terry RD, Morrison JH. Laminar and regional distributions of neurofibrillary tangles and neuritic plaques in Alzheimer's disease: A quantitative study of visual and auditory cortices. *J Neurosci* 1987;**7**:1799–1808.
45. Pearson RC, Esiri MM, Hiorns RW, Wilcock GK, Powell TP. Anatomical correlates of the distribution of the pathological changes in the neocortex in Alzheimer disease. *Proc Natl Acad Sci U S A* 1985;**82**:4531–4534.
46. Van Hoesen GW. Ventromedial temporal lobe anatomy, with comments on Alzheimer's disease and temporal injury. *J Neuropsychiatry Clin Neurosci* 1997;**9**:331–341.
47. Scholtens LH, Schmidt R, de Reus MA, van den Heuvel MP. Linking macroscale graph analytical organization to microscale neuroarchitectonics in the macaque connectome. *J Neurosci* 2014;**34**:12192–12205.
48. Hyman BT, Kromer LJ, Van Hoesen GW. A direct demonstration of the perforant pathway terminal zone in Alzheimer's disease using the monoclonal antibody Alz-50. *Brain Res* 1988;**450**:392–397.
49. Honey CJ, Sporns O, Cammoun L, et al. Predicting human resting-state functional connectivity from structural connectivity. *Proc Natl Acad Sci U S A* 2009;**106**:2035–2040.
50. Johansen-Berg H, Rushworth MF. Using diffusion imaging to study human connectional anatomy. *Annu Rev Neurosci* 2009;**32**:75–94.
51. Jbabdi S, Johansen-Berg H. Tractography: Where do we go from here? *Brain Connect* 2011;**1**:169–183.
52. Greicius MD, Srivastava G, Reiss AL, Menon V. Default-mode network activity distinguishes Alzheimer's disease from healthy aging: Evidence from functional MRI. *Proc Natl Acad Sci U S A* 2004;**101**:4637–4642.
53. Yao Z, Zhang Y, Lin L, Zhou Y, Xu C, Jiang T. Alzheimer's Disease Neuroimaging Initiative. Abnormal cortical networks in mild cognitive impairment and Alzheimer's disease. *PLoS Comput Biol* 2010;**6**:e1001006.
54. Petrella JR, Sheldon FC, Prince SE, Calhoun VD, Doraiswamy PM. Default mode network connectivity in stable vs progressive mild cognitive impairment. *Neurology* 2011;**76**:511–517.
55. Chhatwal JP, Schultz AP, Johnson K, et al. Impaired default network functional connectivity in autosomal dominant Alzheimer disease. *Neurology* 2013;**81**:736–744.

Supporting Information

The following supplementary material is available for this article:

Data S1. Methodological details and additional analyses.

Figure S1. Bar plot showing the percentage of affected connections (in terms of NOS) for the first and second ring in each group of patients when the four strongest hub nodes, having the highest number of connections, (superior parietal and putamen, left and right) were taken as the epicenter. Connectivity disruptions were not found to be stronger in the first ring compared to the second ring, suggesting that hub nodes are not specifically targeted in aMCI and AD as hypothesized by the "nodal stress" model of neurodegeneration. Proportions of affected connections observed in the aMCI/mild AD/moderate AD patient groups were: 3.7 / 8.4 / 17.5% (first ring); 2.8 / 10.4 / 18.8% (second ring).